Published in final edited form as:
J Comput Neurosci. 2010 April ; 28(2): 305–321. doi:10.1007/s10827-009-0210-2.

Synchrony with shunting inhibition in a feedforward inhibitory network

Sachin S. Talathi,
J Crayton Pruitt Family Department of Biomedical Engineering, University of Florida, Gainesville, FL 32611, USA

Dong-Uk Hwang,
Korea Institute of Oriental Medicine, 483 Exporo, Yuseong-gu, Daejeon, 305-811, Republic of Korea

Paul R. Carney, and
J Crayton Pruitt Family Department of Biomedical Engineering, University of Florida, Gainesville, FL 32611, USA

William L. Ditto
School of Biological and Health Systems Engineering, Arizona State University, Tempe, AZ 85287, USA

Sachin S. Talathi: stalathi@bme.ufl.edu; Dong-Uk Hwang: duhwang@gmail.com; Paul R. Carney: carnepr@peds.ufl.edu; William L. Ditto: william.ditto@asu.edu

Abstract

Recent experiments have shown that $GABA_A$ receptor mediated inhibition in adult hippocampus is shunting rather than hyperpolarizing. Simulation studies of realistic interneuron networks with strong shunting inhibition have been demonstrated to exhibit robust gamma band (20–80 Hz) synchrony in the presence of heterogeneity in the intrinsic firing rates of individual neurons in the network. In order to begin to understand how shunting can contribute to network synchrony in the presence of heterogeneity, we develop a general theoretical framework using spike time response curves (STRC's) to study patterns of synchrony in a simple network of two unidirectionally coupled interneurons (UCI network) interacting through a shunting synapse in the presence of heterogeneity. We derive an approximate discrete map to analyze the dynamics of synchronous states in the UCI network by taking into account the nonlinear contributions of the higher order STRC terms. We show how the approximate discrete map can be used to successfully predict the domain of synchronous 1:1 phase locked state in the UCI network. The discrete map also allows us to determine the conditions under which the two interneurons can exhibit in-phase synchrony. We conclude by demonstrating how the information from the study of the discrete map for the dynamics of the UCI network can give us valuable insight into the degree of synchrony in a larger feedforward network of heterogeneous interneurons.

Keywords

Synchrony; Shunting inhibition; Spike time response curve; Arnold tongue; Feed forward network

Correspondence to: Sachin S. Talathi, stalathi@bme.ufl.edusachin.talathi@gmail.com.

1 Introduction

Synchronous rhythms in the brain, in particular gamma rhythms (20–80 Hz) are known to constitute a fundamental mechanism for cognitive tasks such as object recognition (Mima et al. 2001; Baudry and Bertrand 1999), associative learning (Gruber et al. 2001, 2002) and the processing of sensory information in the brain (Engel and Singer 2001; Aoki 1999). A number of *in-vitro* slice experiments have demonstrated that fast inhibitory response mediated by $GABA_A$ receptors are both necessary and sufficient for the generation of sustained gamma-band oscillations in the hippocampus (Whittington et al. 1995; Fisahn et al. 1998; LeBeau et al. 2002; Mann et al. 2005). Early theoretical work by Wang and Rinzel (1992), demonstrating the ability for reciprocally connected interneurons to exhibit synchronous rhythms, provided a mechanistic framework for synchrony exhibited by purely inhibitory neuronal network. In the subsequent years there have been a number of theoretical and simulation studies of synchrony in networks of coupled interneurons (vanVreeswijk et al. 1994; Wang and Buzsaki 1996; Ernst et al. 1995; White et al. 1998; Chow et al. 1998). The primary conclusion from these studies was that while homogeneous networks of inhibitory coupled neurons can exhibit synchrony, it was extremely sensitive to heterogeneity in the network parameters. Most of the earlier theoretical work focused on hyperpolarizing effects of $GABA_A$ mediated fast inhibition. However recent experimental work by Bartos et.al., has demonstrated that $GABA_A$ mediated inhibition in hippocampal slices of adult mammalian brains, is fast and shunting (Bartos et al. 2002; Vida et al. 2006). Through simulation studies on a realistic network model of coupled interneurons, the authors have also demonstrated that shunting enhances robust gamma-band synchrony in the network even in the presence of moderately high heterogeneity (Bartoset et al. 2007). However due to the inherent complexity of the realistic network considered by Bartos et.al, (a large network comprising of 200 interneurons, electrical coupling among neighboring pair of interneurons, the presence of synaptic propagation delay, fast synaptic decay time, strong synaptic conductance) it has been difficult to elucidate the contribution of shunting to the enhancement of synchrony of the network in the gamma-band. Infact recent theoretical work by Jeong and Gutkin (2007) suggests that shunting may enhance stable asynchronous states in the network of coupled interneurons. However the authors note that the observed difference between their results and those obtained by Bartos et.al., may lie in the different regimes of synaptic coupling considered and the lack of heterogeneity in the intrinsic firing rates of the coupled neurons.

Here, we investigate whether the analytical framework of spike time response curves (STRCs) can be used to study synchronous state of 1:1 phase locking between two unidirectionally coupled neurons (UCI network) interacting through a strong shunting synapse in the presence of heterogeneity (Talathi et al. 2009). We begin by demonstrating that synaptic input through shunting inhibition to a neuron periodically firing in the gamma frequency band persists for 3 consecutive firing cycles as opposed to the case for neuron receiving strong synaptic input through a hyperpolarizing synapse. We then develop an analytical framework to approximate the dynamics of 1:1 synchronous state in the UCI network through a discrete map that takes into account the higher order STRC contributions. We show that in the limit of zero higher order STRC contributions the discrete map reduces to the well-known approximation for synchrony between two neurons coupled through a hyperpolarizing inhibitory synapse (Ermentrout 1996; Acker et al. 2004; Talathi et al. 2008). We then use the discrete map to determine the conditions under which in-phase synchrony can be observed in this network. We show that synaptic delays play an important role in the generation of in-phase synchrony between the two coupled interneurons interacting through a shunting synapse. In the spirit of White et al. (1998), we conclude by demonstrating that analysis of smaller networks can be useful in understanding larger network dynamics and

may provide more insight into the results obtained by Bartoset et al. (2007) for a more biologically realistic networks.

2 Methods

2.1 Model

Each neuron is modeled based on a single compartment neuron model developed by Wang and Buzsaki (1996) with a fast sodium channel, a delayed rectifier potassium channel and a leak channel. The dynamical equation for the model neuron is given by,

$$C\frac{dV(t)}{dt}=I^{DC}+g_{Na}m_{\infty}^{3}h(t)(E_{Na}-V(t))+g_{K}n^{4}(t)\,(E_{K}-V(t))+g_{L}(E_{L}-V(t))+I_{S}(t) \quad (1)$$

where $C = 1\mu F/cm^2$. $V(t)$ is the membrane potential, I^{DC}: external DC current, is set such that the neuron spikes at a given intrinsic frequency $F(I^{DC})$. $I_S(t) = g_S S(t)(E_I - V(t))$ is the synaptic current from external inhibition. g_S represents the strength of the synaptic connection. E_r (r = Na, K, L) are reversal potentials of the sodium and potassium ion channels and the leak channel respectively. E_I, is the reversal potential of the inhibitory synapse. g_r (r = Na, K, L) represent the conductance of sodium, potassium and the leak channel respectively. The steady state activation for sodium current $m_\infty = \alpha_m/(\alpha_m + \beta_m)$. The inactivation variable for sodium channel $h(t)$ and the activation variable for potassium current $n(t)$ satisfy the following first order kinetic equation:

$\frac{dX(t)}{dt}=\varphi(\alpha_X(V(t))(1-X(t))-\beta_X(V(t))X(t))$, where $X(t) = h(t), n(t)$ with $\phi = 5$. The functions α_X and β_X are given by:

$$\alpha_m=\frac{-0.1(V(t)+35)}{e^{-0.1(V(t)+35)}-1} \qquad \beta_m=4e^{-(V(t)+60/18)}$$
$$\alpha_h=0.07e^{-(V(t)+58)/20} \qquad \beta_h=\frac{1}{e^{-0.1(V(t)+28)}+1}$$
$$\alpha_n=\frac{-0.01(V(t)+34)}{e^{-0.1(V(t)+34)}-1} \qquad \beta_n=\frac{0.125}{e^{-(V+44)/88}}$$

$S(t)$ gives the fraction of bound receptors and satisfy the following first order kinetic equation, (Abarbanel et al. 2003; Talathi et al. 2008),

$$\dot{S}(t)=\frac{S_0\left(V_{pre}(t)\cdot\theta(t)\right)-S(t)}{\widehat{\tau}\left(S_I-S_0\left(V_{pre}(t)\cdot\theta(t)\right)\right)}$$

where $\theta(t) = \Sigma_i\,\Theta(t - t_i).\Theta((t_i + \tau_r) - t)$. $\Theta(X)$ is the heaviside function satisfying $\Theta(X) = 1$ if $X > 0$ else $\Theta(X) = 0$ and t_i is the time of the i^{th} presynaptic neuronal spike ($V_{pre}(t)$). The kinetic equation for $S(t)$ involves two time constants, $\tau_R = \hat{\tau}(S_I - 1)$, the docking time for the neurotransmitter and $\tau_D = \hat{\tau}S_I$, the undocking time constant for the neurotransmitter binding. Finally, $S_0(\theta)$ is the sigmoidal function given by, $S_0(\theta) = 0.5(1 + \tanh(120(\theta - 0.1)))$.

All the simulations were performed using fixed time step 4^{th} order Runge-Kutta method for differnetial equations with time step $\delta t = 0.05$ ms, on a 2GHz Intel Core Duo Mac OS X. The source code is available from SST on request.

2.2 Spike time response curve (STRC)

As a measure of the influence of synaptic input on the firing times of a neuron, we define the spike time response curves (STRC's) (Acker et al. 2004; Oprisan et al. 2004)

$$\Phi_j(\delta t, \tau_R, \tau_D, g, E_R, T_0) = \frac{T_j(\delta t) - T_0}{T_0}$$

where T_0 is the intrinsic period of spiking, $T_j(\delta t)$ represents the length of the j^{th} spiking cycle in the presence of a single perturbation at time δt. The first spiking cycle $j = 1$ is assumed to start at time $t = 0$ and the neuron is assume to received synaptic perturbation in the first spiking cycle at time $0 < \delta t < T_0$. The synaptic parameters are: τ_R: the synapse rise time, τ_D: the synaptic decay time, g_s: the synaptic strength and E_R: the reversal potential of the synapse. No constraint is placed on the synaptic strength (Ermentrout and Kopell 1990; Bartoset et al. 2007). In addition we assume that the intrinsic period of spiking for the neuron T_0 is constant. We therefore ignore the important case of spike frequency adaptation (Ermentrout et al. 2001). However, more recently Cui et al. (2009) have addressed the issue of spike frequency adaptation using functional phase response curves. The STRC's are obtained numerically as explained through the schematic diagram in Fig. 1(a). The neuron firing regularly with period T_0, is perturbed through an inhibitory synapse at time δt after the neuron has fired a spike at reference time zero. The spiking time for neuron is considered to be the time when the membrane voltage V, crosses a threshold (set to 0 mV in all the calculations presented here). As a result of this perturbation, the neuron fires the next spike at time t_1, representing the first cycle after perturbation of length $T_1 \neq T_0$. Depending on the properties of the synapse, *i.e.*, g_s, τ_R, τ_D and E_R; the length of subsequent cycles might change. In Fig. 1(b-d) we show the first three STRC components Φ_1, Φ_2 and Φ_3 respectively, color coded as function of the reversal potential of the synapse E_R and the perturbation time δt for a given value of $g_s = 0.15\text{mS/cm}^2$, $\tau_R = 0.1$ ms and $\tau_D = 8$ms. As can be seen from Fig. 1(b), the first order STRC is non-zero for all perturbation times $0 < \delta t < T_0$ for the entire range of E_R values, the difference being for hyperpolarizing synapses ($E_R \leq V_{\text{rest}}$), the time to next spike is delayed resulting in positive values for Φ_1 whereas for shunting synapses ($V_{\text{rest}} < E_R \leq V_T$) the time to next spike is advanced resulting in negative values for Φ_1. As can be seen from Fig. 1(c), there is a significant contribution to second order STRC for shunting synapses for all values of $0 < \delta t < T_0$, however for hyperpolarizing synapses, Φ_2 is non-zero only for $\delta t \to T_0$. From Fig. 1(d) we see that for shunting synapses with reversal potential close to spiking threshold ($E_R \approx V_T$), there is contribution to third order STRC term for $\delta t \to T_0$. Higher order STRC terms are non-zero for a neuron receiving synaptic input through a slow shunting synapse because (i) Shunting input depolarizes the membrane potential and as a result the period of firing cycle in which the perturbation is received is decreased (evident from the negative value for Φ_1) (ii) The effect of slow synapse then persists for a larger fraction of the period of first cycle and as a result it modulates the length of second cycle resulting in a significant non-zero contribution to second order STRC. These effects are clearly demonstrated through Fig. 1(a) inset, where we depict the time series of neurons membrane potential and the synaptic variable $S(t)$ for the two cases $E_R = -55$ mV (shunting) and $E_R = -75$ mV (hyperpolarizing). It is clear from the inset that $S(t)$ is non-zero for the first firing cycle and as a result modulates the length of the subsequent cycle.

For all further calculations, unless otherwise mentioned, we will suppress the dependence of STRC on synaptic parameter's: τ_R, τ_D and E_R, g and the intrinsic period of the neuron T_0. For ease of analytical calculations for synchrony between the coupled neuron's we define the following (see Fig. 2(a)).

$$R(\delta t)=T_0(1+\Phi_1(\delta t)) - \delta t \quad (2)$$

$$E_j(\delta t)|_{j>1}=T_0(1+\Phi_j(\delta t)) \quad (3)$$

where $R(\delta t)$ defines the recovery time for the trajectory to generate the next spike following synaptic perturbation at time δt and $E_j(\delta t)$ is the period of j^{th} firing cycle in presence of single perturbation at time δt.

3 Results

3.1 Estimating period of oscillation in the presence of two consecutive synaptic stimuli

We begin by considering the simple case of a periodically firing neuron (with intrinsic period T_0) that receives a $GABA_A$ mediated inhibition through a shunting synapse in each of its two successive firing cycles at times δt_1 and δt_2 as shown in Fig. 2(a). Our goal is to determine the length of the second cycle $T_2(\delta t_1, \delta t_2)$ using the open loop STRC functions Φ_j (j = 1,2,3…) as defined above.

In the presence of a single perturbation at δt_1 in the cycle 1, following from the definition of STRC's we can obtain the length of second cycle as: $T_2(\delta t_1) = E_2(\delta t_1) = T_0 (1 + \Phi_2(\delta t_1))$. It is clearly a function of single perturbation time occurring at time $0 \leq \delta t_1 < T_0$ in the first cycle which begins at time $t = 0$. Similarly in the presence of a single perturbation in cycle 2 at time $T_0 \leq \delta t_2 < 2T_0$, again following from the definition of STRC's we have $T_2(\delta t_2) = \delta t_2 + R(\delta t_2) = T_0(1 + \Phi_1(\delta t_2))$. In writing this equation we made an implicit assumption that the default period of second cycle in the absence of the single perturbation at time δt_2 is T_0. However if the synaptic input at δt_2 is preceded by a synaptic perturbation in the previous cycle at δt_1, the length of the second cycle is no longer T_0. Therefore, in order to correctly determine the length of second cycle in this case, we have to compensate for the change in the length of second cycle caused by synaptic input at time δt_1. This compensation is done by re-normalizing the synaptic perturbation time in the second cycle to $\delta t_2^e=\delta t_2 \frac{T_0}{E_2(\delta t_1)}$ and re-scaling the effective phase of perturbation by $\alpha_2^e=\frac{\delta t_2}{E_2(\delta t_1)} - \frac{\delta t_2}{T_0}$, using the procedure described below and explained schematically using Fig. 2(a).

A synaptic input perturbs the trajectory of periodically firing neuron away from the stable limit cycle attractor. In absence of any further perturbation, the trajectory will asymptotically approach the limit cycle with a constant phase velocity, as a result the neuron returns back to the threshold for firing at time $T_1 \neq T_0$. In Fig. 2(a), this effect is represented by assuming that the trajectory does not move away from the limit cycle, rather the phase velocity of the neuron around the limit cycle is increased uniformly. Since the effect of synaptic perturbation is now treated as changing the phase velocity of the trajectory on the limit cycle, we can use the open loop STRC's to estimate the effective period of the cycle receiving the synaptic perturbation. Our assumption of change in phase velocity however implies that the intrinsic period of oscillation of the trajectory on the limit cycle is modified and as a result the shape of STRC (plotted as a function of the time of synaptic perturbation, see Fig. 1) which clearly depends on the intrinsic period of oscillator will change. Depending on whether $E_2(\delta t_1) > T_0$ or $E_2(\delta t_1) < T_0$, the STRC will either be stretched or compressed along the time axis. We assume that this scaling is linear and compensate for the change in shape of STRC along the time axis by re-normalizing the effective time of

synaptic perturbation δt_2 to δt_2^e using similar triangles property applied to three distinct triangles in the phase plot depiction of the phenomenon sketched in Fig. 2(a). Triangle 1 (shown in inset of Fig. 2(a)) implies δt_2 is to $E_2(\delta t_1)$ as x is to 1. This gives $x = \delta t_2/E_2(\delta t_1)$. The second triangle implies that δt^e is to x as T_0 is to 1. Therefore we get $\delta t_2^e = xT_0$ or as stated above, $\delta t_2^e = \delta t_2 \frac{T_0}{E_2(\delta t_1)}$. Thus the re-normalization of the effective perturbation time accounts for the rescaling of the STRC along the time axis due to the change in phase velocity of the trajectory. However the change in phase velocity of the trajectory also means that the neuron is receiving different amount of current for a given magnitude of synaptic perturbation. This is because the speed of the trajectory along the limit cycle depends on the net current delivered to the neuron. This is especially true for type-I neuron models, for which a single synaptic perturbation either delays (for inhibitory synaptic input) or advances (excitatory synaptic input) the time to next spike (Gutkin et al. 2004; Ermentrout 1996).

Thus, in order to correctly account for the true effect of the perturbation on the original trajectory, we also have to rescale the effective magnitude of the synaptic perturbation. Going back to the Fig. 2(a), applying similar triangles property to triangle 3, this rescaling is done by modifying the effective phase of synaptic perturbation by α_2^e. From triangle 3 we see that δt_2 is to T_0 as $x - \alpha_2^e$ is to 1. Therefore we get $\alpha_2^e = x - \delta t_2/T_0$ or as described above $\alpha_2^e = \frac{\delta t_2}{E_2(\delta t_1)} - \frac{\delta t_2}{T_0}$. The change in effective magnitude of synaptic perturbation will now change the amount of time it takes for the neuron to return back to its stable limit cycle oscillator, thereby changing the amount of recovery time. Analytical expression for the resulting modification to recovery time was obtained by empirically fitting the recovery time of the trajectory to the rescaled amplitude of the synaptic perturbation. We found that the best fit in the least-squares sense, to the resulting recovery time can be obtained by rescaling the recovery time $R(\delta t_2^e)$ to $R(\delta t_2^e)(1 - \alpha_2^e)$. While this expression was found through empirical fitting procedure, we have tested the generality of this modification by performing similar calculations on a different model for type-1 neurons, the Morris-Lecar oscillator.

Thus, the re-normalization of the perturbation time and the re-scaling of the effective magnitude of synaptic perturbation and the resulting recovery time interval, allows us to correctly account for the effect of synaptic input at time δt_1 on the length of cycle 2. The length of cycle 2, which is now a function of δt_1 and δt_2, can now be written as

$$\begin{aligned} T_2(\delta t_1, \delta t_2) &= \delta t_2 + R(\delta t_2^e) \cdot (1 - \alpha_2^e) \\ &= \delta t_2 + \left[T_0 \left(1 + \Phi_1 \left(\delta t_e^2\right)\right) - \delta t_e^2 \right] \times \left(1 - \frac{\delta t_2}{E_2(\delta t_1)} + \frac{\delta t_2}{T_0}\right) \\ &= \delta t_2 + \left[T_0 \left(1 + \Phi_1 \left(\frac{\delta t_2}{1+\Phi_2(\delta t_1)}\right)\right) - \frac{\delta t_2}{1+\Phi_2(\delta t_1)} \right] \times \left(1 - \frac{\delta t_2}{T_0(1+\Phi_2(\delta t_1))} + \frac{\delta t_2}{T_0}\right) \end{aligned} \quad (4)$$

In order to determine the set of $\{\delta t_1, \delta t_2\}$ for which Eq. (4) holds, we have estimated $T_2(\delta t_1, \delta t_2)$ by solving Eq. (1) numerically for the situation when the neuron receives synaptic input through $GABA_A$ mediated synapse that is shunting (with parameters: $\tau_R = 0.2$ ms, $\tau_D = 8$ ms, $g_M = 0.1$ mS/cm^2 and $E_R = -55$ mV) and compared the numerically obtained result with that determined through Eq. (4), using the values of STRC's Φ_1 and Φ_2. In Fig. 2(b), we show results in the form of two dimensional plot of δt_1 versus δ_2, with the color representing the percent error $\delta E_2 = 100 \frac{|T_2^N - T_2^P|}{T_2^N}$; where T_2^N represents the numerically estimated period $T_2(\delta t_1, \delta t_2)$ by solving Eq. (1), while T_2^P represents the length of $T_2(\delta t_1, \delta t_2)$ estimated

through STRC's using Eq. (4). In Fig. 2(c), we show the results for a specific case of δt_1 = 15 ms. We see that by correctly taking into account the nonlinear contributions from the second order STRC term Φ_2 through the re-normalization and re-scaling technique, the STRC's contain all the information required to predict the length of second cycle in the presence of two consecutive synaptic perturbations.

Let us now consider two special cases commonly considered in the analysis of neuronal network synchrony using STRC's: (a) $\Phi_2(\delta t) = 0$ and (b) non-zero $\Phi_2(\delta t)$ for $\delta t \rightarrow T_0$; as in the case of hyperpolarizing synapse with slow decay time (Fig. 1(b)). For the first case, Eq. (4) simply reduces to $T_2(\delta t_1, \delta t_2) = T_0 (1 + \Phi_1(\delta t_2))$, where the period in second cycle in not affected by perturbation in the first cycle and is completely determined through the first order STRC term Φ_1. In the second case, linearization of Eq. (4) results in

$$T_2(\delta t_1, \delta t_2) \approx T_0(1+\Phi_1(\delta t_2)+\Phi_2(\delta t_1)) \tag{5}$$

As stated above, Eq. (5) results from first order correction from Φ_2 to the length of second cycle in presence of two consecutive synaptic perturbations. Under the assumption that the second order resetting dies out, which is mostly likely in the situation that $\Phi_2(\delta t) \approx 0$ unless $\delta t \rightarrow T_0$, the approximation in the form given in Eq. (5) has been used in Oprisan and Canavier (2001) to determine the effect of second order STRC component on stability of 1:1 synchronous state in a ring of pulse coupled oscillators; in Oprisan et al. (2004) to determine phase resetting and phase locking in a hybrid circuit of one model neuron and one biological neuron and also recently in Maran and Canavier (2008) to predict 1:1 and 2:2 synchrony in mutually coupled network of interneurons with synapse that is hyperpolarizing. We emphasize that in the works cited above the application of Eq. (5) which we obtain as linearization of Eq. (4) for the situation of only two consecutive pulses, is successfully applied to the situation when the two neurons are locked in stable 1:1 synchrony, i.e., periodic perturbation such that the trajectory of a perturbed neuron always returns to its limit cycle before the occurrence of the subsequent perturbation. If the above approximation is applied to the case considered in this section, i.e., two consecutive pulses only, it is able to predict the length of second cycle for hyperpolarizing synapse (see Fig. 3(a)), however, there is a significant prediction error as quantified through $\delta E_2 = 100\frac{|T_2^N - T_2^P|}{T_2^N}$ when Eq. (5) is used to obtain an estimate T_2^P for $T_2(\delta t_1, \delta t_2)$ when the neuron receives two successive perturbations through a shunting synapse (see Fig. 3(b)), in which case the second order resetting is significantly non-zero and the trajectory fails to return to the limit cycle before the application of the second synaptic perturbation. If we assume that indeed the second order resetting is complete before the arrival of second pulse at time δt_2, the effective period of second cycle would be

$$T_2(\delta t_1, \delta t_2)=T_0(1+\Phi_1(\delta t_2 - T_0\Phi_2(\delta t_1))) \tag{6}$$

As shown in Fig. 3(c), this assumption breaks down for the case of shunting synapse. We thus see that while Eq. (4) correctly predicts the length of second cycle $T_2(\delta t_1, \delta t_2)$ for a neuron receiving two successive synaptic perturbations through a shunting synapse, both Eq. (5) which results from linearization of Eqs. (4) and (6) which results from the assumption that second order resetting is complete before the arrival of second synaptic perturbation, fail to capture the non-linear contribution from the higher order STRC term in determining $T_2(\delta t_1, \delta t_2)$. We emphasize that the expression for the predicted value of $T_2(\delta t_1, \delta t_2)$ through

Eq. (4) is only dependent on STRCs estimated for a given synapse type without any explicit assumption on the strength of synaptic input to the neuron and is valid both in the regime of weak and strong coupling and for slow and fast synaptic dynamics.

3.2 Estimating period of oscillation in the presence of three consecutive synaptic stimuli

We can now generalize our approach to consider the situation when the neuron receives synaptic inputs in 3 consecutive firing cycles: δt_1 in cycle 1; δt_2 in cycle 2 and δt_3 in cycle 3. This is an important case to consider in order to derive a return map for 1:1 synchrony between two mutually coupled interneurons through $GABA_A$ synapse that is shunting; since we know from Fig. 1(b–d); the first 3 STRC components are non-zero for shunting inhibition. We first determine the length of third cycle $\tilde{E}_3(\delta t_1, \delta t_2)$, when the neuron receives two synaptic inputs at times δt_1 and δt_2. Since $\Phi_3(\delta t) \approx 0$ (see Fig. 1(d)), following Eq. (5) we can approximate $\tilde{E}_3(\delta t_1, \delta t_2) \approx T_0\left(1+\Phi_2(\delta t_2^e)+\Phi_3(\delta t_1)\right)$. In Fig. 4(a), the percent error $\delta\tilde{E}_3(\delta t_1, \delta t_2)=100\left|\frac{\tilde{E}_3^N-\tilde{E}_3^P}{\tilde{E}_3^N}\right|$ between the empirically estimated $\tilde{E}_3^P$ using STRC's and those obtained through numerical simulations $\tilde{E}_3^N$ is color coded as function of δt_1 and δt_2. Now, following from Eq. (4), the length of 3rd cycle in the presence of three consecutive synaptic inputs can be written as: $T_3(\delta t_1, \delta t_2, \delta t_3) \approx \delta t_3+R(\delta t_3^e).(1-\alpha_3^e)+T_0\Phi_3(\delta t_1)$; where $\delta t_3^e=\delta t_3\frac{T_0}{\tilde{E}_3(\delta t_1, \delta t_2)}$ and $\alpha_3^e=\frac{\delta t_3}{\tilde{E}_3(\delta t_1, \delta t_2)}-\frac{\delta t_3}{T_0}$. Note the addition of the term $T_0\Phi_3(\delta t_1)$, which determines the contribution of the first spike to the third cycle. First order linear correction to $T_3(\delta t_1, \delta t_2, \delta t_3)$ through Φ_3 is justified by our consideration of $T_2(\delta t_1, \delta t_2)$ with first order linear correction through Φ_2 in Eq. (5). As we showed earlier first order linear correction term through Φ_2 when it satisfies the condition $\Phi_2(\delta t) \approx 0$ unless $\delta t \to T_0$ provides a good approximation for estimating $T_2(\delta t_1, \delta t_2)$, in situation when $\Phi_3 \approx 0$ except when $\delta t \to 0$, the contribution to $T_3(\delta t_1, \delta t_2, \delta t_3)$ from the third order correction term can also be approximated through a first order linear correction. We therefore have

$$\begin{aligned} T_3(\delta t_1, \delta t_2, \delta t_3) &\approx \delta t_3+\left[T_0\left(1+\Phi_1(\delta t_3^e)\right)-\delta t_3^e\right]\cdot(1-\alpha_3^e)+T_0\Phi_3(\delta t_1) \\ &=\delta t_3+\left[T_0\left(1+\Phi_1\left(\frac{T_0\delta t_3}{\tilde{E}_3(\delta t_1,\delta t_2)}\right)\right)-\frac{T_0\delta t_3}{\tilde{E}_3(\delta t_1,\delta t_2)}\right]\times\left(1-\frac{\delta t_3}{\tilde{E}_3(\delta t_1,\delta t_2)}+\frac{\delta t_3}{T_0}\right)+T_0\Phi_3(\delta t_1) \end{aligned} \quad (7)$$

In Fig. 4(b), we show the error between the empirically estimated T_3^P obtained from Eq. (6) above, and the numerically determined length of third cycle T_3^N by solving Eq. (1) through the color coded percent error $\delta E_3(\delta t_1, \delta t_2)|=100\left|\frac{T_3^N-T_3^P}{T_3^N}\right|$ plot for the specific case of δt_3 = 5 ms. We again see that through the procedure of re-normalization and re-scaling STRC's contain all the information necessary to predict the length of third cycle $T_3(\delta t_1, \delta t_2, \delta t_3)$ resulting from synaptic perturbations in three consecutive firing cycles.

3.3 Return map for 1:1 synchrony between coupled interneurons

We are now in the position to derive the discrete map for 1:1 phase locked state (1:1 synchrony) between two unidirectionally coupled interneurons interacting through a shunting synapse in the UCI network as shown in Fig. 5(a). In absence of an external synaptic drive, neuron A fires with intrinsic period T_0^A in response to current input I_{DC}^A. Let

neuron B receive input current $I_{DC}^{B}=I_{DC}^{A}\left(1+\frac{H}{100}\right)$, where H represents the percent heterogeneity. For $H \neq 0$, neuron B fires with intrinsic period $T_0^B \neq T_0^A$. When the two neuron are locked in 1:1 synchrony we have from Fig. 5(b) and Eq. (7)

$$t_{n+1}^{A} \approx t_n^A+\delta_n+R^A\left(\delta_n\frac{T_0^A}{\tilde{E}_3(\delta_{n-2},\delta_{n-1})}\right)\times\left(1-\alpha_3^{eA}(\delta_{n-2},\delta_{n-1})\right)+T_0^A\,\Phi_3^A(\delta_{n-2}) \tag{8}$$

where t_n^X is the time of n^{th} spike for neuron X, $\delta_n=t_n^B-t_n^A$ and the function's R^X and α_3^{eX}, $X = \{A, B\}$ are given through STRC estimates $\Phi_j^X\ (j=1\ldots3)$ obtained for neuron's A and B which are dependent on their intrinsic firing rates T_0^A and T_0^B respectively. Since neuron B, does not receive any external perturbation, we have for neuron B, $t_{n+1}^B=t_n^B+T_0^B$. The discrete map for the evolution of δ_n can then be obtained as:

$$\delta_{n+1} \approx T_0^B-R^A\left(\delta_n\frac{T_0^A}{\tilde{E}_3(\delta_{n-2},\delta_{n-1})}\right)\times\left(1-\alpha_3^{eA}(\delta_{n-2},\delta_{n-1})\right)-T_0^A\,\Phi_3^A(\delta_{n-2}) \tag{9}$$

Equation (9) represents a 3-dimensional nonlinear discrete map for the evolution of variables: $\{\delta_n,\alpha_n,\beta_n\}$ given by:

$$\begin{aligned}\delta_{n+1} &\approx T_0^B-R^A\left(\delta_n\frac{T_0^A}{\tilde{E}_3(\beta_n,\alpha_n)}\right)\cdot\left(1-\alpha_3^{eA}(\beta_n,\alpha_n)\right)-T_0^A\,\Phi_3^A(\beta_n)\\ \alpha_{n+1}&=\delta_n\\ \beta_{n+1}&=\alpha_n\end{aligned} \tag{10}$$

The steady state solution to above equation can be obtained by solving for the fixed point δ^* defined by $\delta_{n+1} = \alpha_{n+1} = \beta_{n+1} = \delta_n = \alpha_n = \beta_n = \delta^*$. We then obtain $F(\delta^*)=T_0^B$, where $F(\delta^*)$ is given by

$$F(\delta^*) \approx \delta^*+T_0^A\,\Phi_3(\delta^*)+R\left(\frac{\delta^*T_0^A}{\tilde{E}_3(\delta^*,\delta^*)}\right)\times\left(1-\frac{\delta^*}{\tilde{E}_3(\delta^*,\delta^*)}+\frac{\delta^*}{T_0^A}\right) \tag{11}$$

In the limit of $\Phi_2 \approx 0$ and $\Phi_3 = 0$, $F(\delta^*) \approx T_0^A\,(1+\Phi_1(\delta^*)+\Phi_2(\delta^*))$ corresponding to the well-known equation for the solution to the fixed point of discrete map for 1:1 synchrony between two neurons coupled through a hyperpolarizing synapse (Talathi et al. 2008). Stability of the fixed point δ^* can be determined through linear stability analysis for discrete dynamical systems (Strogatz 2001), by calculating the eigenvalues λ_j ($j = 1\ldots3$) of the Jacobian matrix for Eq. (9). Stability implies $|\lambda_j| < 1$.

In order to determine whether Eq. (10) can predict 1:1 phase locked states for the UCI network considered above, we consider the specific case of neurons A and B coupled through a slow shunting synapse with parameters: $E_R = -55$ mV, $\tau_R = 0.1$ ms, and $\tau_D = 8$

ms. Neuron A receives fixed dc current I_{DC}^{A}, such that fires with intrinsic period T_0^A=31 ms. We solve Eq. (11), for different values of H, thereby modulating T_0^B, to determine the set of values for g_s, which will result in stable fixed point solution for Eq. (11). The solution is obtained by estimating STRC's for each value of g_s and then determining whether there is a fixed point solution to Eq. (11). In Fig. 5(c), we present the results of this calculation. For a given value of H, the curve in black gives the lower and upper bounds on the strength of coupling for shunting synapse g_s, for which a unique stable solution to Eq. (11) exists. Stability of the fixed point solution to Eq. (11) is determined by calculating the eigenvalues of the Jacobian matrix for the discrete map in Eq. (10). For example with H = 50, the range of values for g_s for which a unique stable solution exists for Eq. (11) is $0.09 < g_s < 0.21$. This region of 1:1 synchronous locking is analogous to the classic Arnold tongue (Kurths et al. 2001; Talathi et al. 2008), obtained for synchrony between two coupled nonlinear oscillators. Arnold tongue provides a two dimensional visualization of this dependence, as a bounded domain of region in the heterogeneity (H)-coupling strength (g) plane, where 1:1 synchrony between the two oscillators exist. For zero strength of coupling, the two heterogeneous oscillators are oscillating at their intrinsic frequencies, that differ from each other for heterogeneity $H \neq 0$. As a result the width of synchrony at zero coupling is zero. As the strength of coupling increases, the range of heterogeneity over which the two coupled oscillators can synchronize increases, resulting in a tongue shaped two dimensional domain. In Fig. 5(c), the general feature of the Arnold tongue is represented as the region bounded by two black curves obtained through STRC by solving for fixed point of Eq. (10). In Fig. 5(c), shown in blue is a similar bound on the range of heterogeneity leading to synchronous oscillations between the two coupled neurons, obtained by numerically solving Eq. (1) for the evolution of the dynamics of the coupled neuron network. This curve is obtained by fixing the firing period of neuron A, T_0^A and varying the firing period of neuron B, by changing I_{DC}^{B} and determining the strength of synaptic coupling g_s that results in $\frac{T_0^B}{\langle T^A \rangle} \approx 1$. As can be seen from Fig. 5(c), the results match to those obtained through STRC calculations for fixed point of Eq. (10). In Fig. 5(d), we present similar calculation for the two neurons coupled through a fast shunting synapse with parameters: $E_R = -55$ mV, $\tau_D = 2$ ms, and $\tau_R = 0.1$ ms.

We note that the Arnold tongue showed in Fig. 5(c) and d are skewed to the right; i.e., $H > 0$, which suggests that shunting inhibition tends to promote 1:1 synchrony at higher frequencies of the driver neuron. Recently Talathi et al. (2008) have demonstrated the mechanism for phase locked state of 1:1 synchrony to exhibit identical synchrony (zero phase lag), which is essential for the generation of synchronous oscillations in a larger network of neurons. It is therefore very likely that through the mechanism of spike timing dependent plasticity (Talathi et al. 2008), the two neurons may lock in identical synchrony (phase locked with zero phase difference) at frequencies in the gamma range. This may result in the generation of gamma oscillations in larger network of interneurons interacting through shunting inhibition as has been demonstrated through simulation studies of realistic networks of neurons (Bartoset et al. 2007). In the next section we test this idea by using the discrete map in Eq. (10) to determining the conditions under which shunting inhibition between the two unidirectionally coupled interneurons can result in inphase synchrony.

3.4 Inphase synchrony with shunting inhibition

In order to determine whether shunting can result in in-phase synchrony, we analyze the discrete map in Eq. (10) to determine the condition for the existence and stability of fixed point $\delta^* = 0$ which represents the state of in-phase synchronous oscillations by the two

heterogeneously firing interneurons in the UCI network. From Eq. (10) we have $\delta_n = \alpha_n = \beta_n = \delta^* = 0$, resulting in

$$\frac{T_0^B}{T_0^A} = 1 + \Phi_1^A(0) \tag{12}$$

In Fig. 6(a), the red circles represent the solution to Eq. (12) in the two dimensional g_s-H plane for the two neurons coupled through a slow-shunting synapse. We see that the solution to fixed point equation for inphase synchrony lies outside the domain for 1:1 synchrony between coupled neurons, suggesting that inphase synchrony is not possible between coupled neurons interacting through slow-shunting synapse. In Fig. 6(b), we show a similar curve represented by red circles for the two neurons coupled through fast-shunting synapse. We see that there exist set of points within the domain for 1:1 synchrony between coupled neurons. However for the coupled neurons to exhibit inphase synchrony, not only should these points be inside the Arnold's tongue but they should also represent stable fixed point solutions to Eq. (10). The stability of these fixed points can be determined through linear stability analysis methodology discussed in Section 3.3, resulting in the following condition:

$$S = T_0^A \frac{d\Phi_1^A(x)}{dx}|_{x=0} + \Phi_2^A(0) \cdot \left(2 + \Phi_1^A(0)\right) > 0 \tag{13}$$

In Fig. 6(c) we plot S, calculated at points representing the solution to Eq. (12) (red circles in Fig. 6(b)) for the fast-shunting synapse, as function of g_S and H. We see that $S < 0$ for all these points, thus Eq. (13) is not satisfied for any pair of g_S-H values, a necessity for the existence of stable inphase solution to the discrete map in Eq. (10). Thus, even for the neuron pair, interacting through a fast-shunting synapse in the UCI network, stable inphase synchronous solution does not exist.

In Fig. 7(a) we demonstrate a possible mechanism for the network considered above to exhibit inphase synchrony. We plot δ_n; defined through:

$$\delta_n = \begin{cases} T_0^B \cdot \mathrm{mod}\left(\frac{t_n^B - t_n^A}{t_{n+1}^B - t_n^B}\right), & \text{if } H < 0; \\ T_0^B \cdot \mathrm{mod}\left(\frac{t_n^B - t_n^A}{t_{n+1}^A - t_n^A}\right), & \text{if } H \geq 0; \end{cases}$$

as function of H for the specific case of a fast shunting shunting synapse with coupling strength $g_s = 0.15$ mS/cm^2. When the two neurons are locked in 1:1 synchrony, $\delta_n \rightarrow \delta^*$, corresponding to the solution of discrete map in Eq. (10) with $\delta_n = 0$ representing inphase synchrony. Shown in black are the results from numerical simulations, and shown in red is the stable solution to the discrete map in Eq. (10). If we introduces synaptic delay $\tau_s = \delta^*$, for a given level of heterogeneity H, we can induce inphase synchrony between the coupled neurons as shown in Fig. 7(b). We see that with $\tau_s = 12$ ms, corresponding to the stable fixed point δ^* for $H = 20\%$, we obtain $\delta_n = 0$ representing the state of inphase synchronous oscillations by the two heterogeneously firing neurons.

In conclusion, for a pair of heterogeneously firing interneurons coupled through a shunting synapse, the two conditions that need to be satisfied for observing inphase synchrony are (i)

the strength of coupling should be such that the coupled oscillators are within the Arnold tongue and (ii) there exists synaptic delay such that the system exhibit's inphase synchrony within the Arnold tongue.

3.5 Synchrony in a feedforward network of inhibitory neurons

In this section, we consider a feed-forward network of 3 heterogeneously firing neurons coupled through a shunting synapse, and demonstrate the utility for the discrete map in determining conditions underwhich this simple network can exhibit inphase synchrony. The network is carefully designed such that each pair of interacting neurons is locally within the Arnold tongue for 1:1 synchrony, for example, $I_{DC}^{0}=0.9113\,\mu$A/cm^2 and $I_{DC}^{1}=0.675\,\mu$A/cm^2 resulting heterogeneity H_{AB} = 35% and for synaptic strength g_s = 0.15 mS/cm^2, the pair oscillates within the Arnold tongue for 1:1 synchrony (see Fig. 5(c)). Thus locally each pair 0–1, 1–2 and 2–0 are within the domain for 1:1 synchrony. As can be seen from Fig. 8(a), even though locally each pair of neurons in the network is within their respective Arnold tongue, the network does not exhibit synchrony when the synaptic delay $\tau_s^{ij}=0$ {i, j=1, 2, 3}. This is because, the neurons are not necessarily phase locked in inphase synchrony. The lag δ* between the firing times of the two neuron phase locked in 1:1 synchrony for a given level of heterogeneity H can be determined using the discrete map in Eq. (9). In Fig. 8(b), we introduce the synaptic delays, derived from the solution to the discrete map in Eq. (9), for a given pair of heterogeneously coupled neurons in the network. By choosing $\tau_s^{01}=12.16$ ms, corresponding to the solution to Eq. (9) for the isolated pair of coupled neurons 0 and 1, through the mechanism discussed in last section, neuron 1 can fire inphase with neuron 0. Similar analysis for the pair of neurons 0 and 2 result in $\tau_s^{02}=1.98$ ms. In isolation, neuron 2 will now be entrained to fire inphase with neuron 0. However in the network considered, neuron 2 also receives synaptic input from neuron 1. If we choose, $\tau_s^{12}=\tau_s^{02}=1.98$ ms, neuron 2 will receive synaptic input from the two distinct neurons 0 and 1 at the same time, as neuron 1 is already entrained to fire inphase with neuron 0. As can be seen from Fig. 8(b), the 3 neurons are now firing in inphase synchrony. Thus using discrete map and pair wise analysis of the coupled neurons in the network we were able to determine the conditions under which the feed-forward network of 3 heterogeneously firing neurons can exhibit synchronous oscillations. Similar analysis can be carried out for a larger feed-forward network ($N > 3$) to determine whether it can exhibit synchronous oscillations.

4 Discussion

In this work we have presented a general mathematical framework to analyze patterns of synchrony in a simple feed-forward network of heterogeneously firing neurons interacting through a shunting synapse. Our work is motivated from the recent experimental findings by Bartoset et al. (2007), demonstrating the ability for a realistic interneuronal network to exhibit robust gamma-band synchrony through shunting synapse in the presence of heterogeneity. Our work is an extension of the theoretical analysis by Jeong and Gutkin (2007) in that we consider the more general case of two neurons coupled through a strong shunting synapse in the presence of heterogeneity. By considering a more simpler situation of uni-directionally coupled neurons, we demonstrate that the results of Jeong and Gutkin pretty much hold true even in the presence of strong-shunting synapse with heterogeneity. In absence of delays in the synaptic transmission, both slow and fast shunting fail to exhibit inphase synchrony between unidirectionally coupled interneurons. The applicability of our methodology as presented in this paper to study patterns of synchrony emerging in a more realistic neuronal network such as considered by Bartoset et al. (2007) remains a topic of future investigation.

The mathematical framework presented in this work is based on the technique of phase reduction which is commonly employed in the study of pulse coupled oscillators (Winfree 2001; Murray 1993). The technique involves determining the phase response curve (PRC) for an oscillator that quantifies how the oscillator responds to a perturbation through a pulsatile input. The PRC for a neuron receiving synaptic perturbations is measured in terms of time rather than phase (Acker et al. 2004) and is referred to as the spike time response curve (STRC). The STRC's provide a natural experimental framework to study the perturbation effects of synaptic inputs on the firing times of a neuron without the requirement of a detailed biophysical model to mimic the neuronal dynamics. We want to emphasize this point by noting that experimental neuroscientists interested in network synchrony do not necessarily know all the ion channels that comprise a neuronal membrane. However it is relatively easy to stimulate a neuron and measure the response time of the neuronal firing and thereby create an experimental log of the effect of synaptic perturbation on a regularly spiking neuron. Once STRC's are determined as described above in the open loop setting, the framework we presented in this work can be used to analyze local synchrony between coupled neurons and in the special case of feed-forward network of inhibitory neurons, make predictions about network synchrony.

We began by demonstrating that STRC's are in general a function of synaptic parameters and for a given level of synaptic strength and synaptic kinetics, the effect of synaptic input varies depending on the form of synaptic inhibition, i.e., hyperpolarizing vs. shunting. For hyperpolarizing synapse, the dominant effect of synaptic perturbation is on the firing cycle that receives the perturbation. However for shunting inhibition, the perturbation effect persists beyond the cycle in which the neuron receives the synaptic perturbation. We found that the analytical technique of re-normalization and re-scaling allowed us to correctly account for the contributions from the higher order STRC terms to the instantaneous firing period of a neuron receiving synaptic input in multiple successive firing cycles. The main advantage of this technique is that it does not require the neuron to approach its intrinsic period of oscillation before receiving the next synaptic perturbation. As a result this technique allowed us to approximate the network dynamics of two heterogeneously firing neurons coupled through a shunting synapse through a discrete map that has the ability to predict the stability of patterns of synchrony in the network. The discrete map also allowed us to determine the conditions under which a larger feed-forward network of heterogeneously firing interneurons can exhibit inphase synchrony. Although in this work we restrict our analysis to the study of feedforward networks, the analytical framework we developed here is equally applicable to study patterns of synchrony generated by a pair of mutually coupled neurons (Talathi et al. 2009). Discrete map analysis for mutually coupled neurons is in particular more challenging. For a given level of heterogeneity, one has to determine STRC's for both neurons in the coupled network (each neuron firing with its own intrinsic period) in order to obtain a discrete map similar to Eq. (10). However once the STRC's are known, one can follow the methodology presented in this work to determine a nonlinear discrete map, stability of the fixed point solution of which can then predict the existence of 1:1 synchronous states (Talathi et al. 2009).

While the methodology that we present in this work enables one to carefully design neuronal networks that can exhibit complete synchrony, the question remains whether such an artificial construction of a neuronal network has any biological relevance. In particular is there a biological mechanism for altering the effective delay in signal propagation between coupled neurons? One particularly relevant pathophysiological scenario that leads to a hypersynchrony of brain networks is the mossy fiber sprouting, which triggers a synaptic reorganization in the dentate gyrus of patients and animal models of temporal lobe epilepsy (Dudek and Shao 2004). The axons of the dentate gyrus excitatory granule cells, develop collaterals that grow into the dentate gyrus molecular layer. A commonly acceptable

hypothesis for seizure generation in patients with temporal lobe epilepsy is that the mossy fiber sprouting trigger hypersynchrony by forming recurrent excitatory connections between the granule cells. It may well be that the modification in the axonal fibers synapsing onto the granule cell bodies may alter the effective delay in the propagation of recurrent excitatory signal and by the mechanisms we propose in this work, trigger a hypersynchronous brain state that eventually leads to the generation of a spontaneous epileptic seizure. More recently there has been a growing interest in controlling the geometry of cell cultures in multielectrode array systems to utilize specially constructed neuronal circuits for various computational tasks such as logic operations (Wolf and Geisel 2008). In the same spirit one can envision the construction of a specialized neuronal circuitry that is tuned to oscillate in synchrony. Such a neuronal circuitry can then be utilized to understand the mechanisms and function of neural synchrony in computation such as the binding problem (Sejnowski 1986). More over different pharmacological drugs can be devised to alter the effective delay in synaptic propagation to break the network synchrony and there by provide an effective control over runaway hypersynchronous brain states that trigger epileptic seizures.

In conclusion, we found that in the feed-forward network of interneurons coupled through a strong shunting synapse, synaptic delays play a critical role in the generation of synchronous oscillations. Another important criteria for the observation of synchrony in a large feed-forward network is the the requirement for local pair of interneurons to be within the Arnold's tongue for 1:1 synchrony. The ability for the framework developed here in determining the synchronizability of a realistic interneuronal network in the presence of heterogeneity as those considered by Bartos et.al., remains a topic of future investigation.

Acknowledgments

This work has been supported in part through a grant from the Office of Naval Research (Grant Number N00014-02-1- 1019), the National Institute of Biomedical Imaging and Bioengineering through Collaborative Research in Computational Neuroscience (R01EB004752) and (EB007082) and the Wilder Center of Excellence for Epilepsy Research at the University of Florida. We acknowledge Dr P. Khargonekar, Dr H. Abarbanel and the anonymous reviewer's for their valuable comments and suggestions on this manuscript.

References

Abarbanel H, Gibb L, Huerta R, Rabinovich M. Biophysical model of synaptic plasticity dynamics. Biological Cybernetics 2003;89:214–226. [PubMed: 14504940]

Acker C, Kopell N, White J. Synchronization of strongly coupled excitatory neurons:relating network behavior to biophysics. Journal of Computational Neuroscience 2004;15:71–90. [PubMed: 12843696]

Aoki F. Increased gamma-range activity in human sensorimotor cortex during performance of visuomotor tasks. Clinical Neurophysiology 1999;110:524–537. [PubMed: 10363776]

Bartos M, Vida I, Frotscher M, Meyer A, Monyer H, Geiger J, et al. Fast synaptic inhibition promotes synchronized gamma oscillations in hippocampal interneuron networks. Proceedings of the National Academy of Sciences 2002;99:13,222–13,227.

Bartos M, Vida I, Jonas P. Synaptic mechanisms of synchronized gamma oscillations in inhibitory interneuron networks. Nature Reviews Neuroscience 2007;8:45–56.

Baudry C, Bertrand O. Oscillatory gamma activity in humans and its role in object representation. Trends in Cognitive Sciences 1999;3:151–161. [PubMed: 10322469]

Chow C, White J, Ritt J, Kopell N. Frequency control in synchronized networks of inhibitory neurons. Journal of Computational Neuroscience 1998;5:407–420. [PubMed: 9877022]

Cui J, Canavier C, Butera R. Functional phase response curves: A method for understanding synchronization of adapting neurons. Journal of Neurophysiology 2009;102:387–398. [PubMed: 19420126]

Dudek F, Shao L. Mossy fiber sprouting and recurrent excitation: Direct electrophysiological evidence and potential implications. Epilepsy Currents 2004;4:184–187. [PubMed: 16059495]

Engel A, Singer W. Temporal binding and the neural correlated of sensory awareness. Trends in Cognitive Sciences 2001;5:16–25. [PubMed: 11164732]

Ermentrout B. Type 1 membranes, phase resetting curves and synchrony. Neural Computation 1996;8:979–1001. [PubMed: 8697231]

Ermentrout B, Kopell N. Oscillator death in systems of coupled neural oscillators. SIAM Journal on Applied Mathematics 1990;50:125–146.

Ermentrout B, Pascal M, Gutkin B. The effect of spike frequency adaptation and negative feedback on the synchronization of neural oscillators. Neural Computation 2001;13:1285–1310. [PubMed: 11387047]

Ernst U, Pawelzik K, Geisel T. Synchronization induced by temporal delays in pulse-coupled oscillators. Physical Review Letters 1995;74:1570–1573. [PubMed: 10059062]

Fisahn A, Pike F, Buhl E, Paulsen O. Cholinergic induction of network oscillations at 40 hz in the hippocampus *in vitro*. Nature 1998;394:186–189. [PubMed: 9671302]

Gruber T, Keil A, Muller M. Modulation of induced gamma band responses and phase synchrony in a paired associate learning task in the human eeg. Neuroscience Letters 2001;316:29–32. [PubMed: 11720771]

Gruber T, Muller M, Keil A. Modulation of induced gamma band responses in a perceptual learning task in the human eeg. Journal of Cognitive Neuroscience 2002;14:732–744. [PubMed: 12167258]

Gutkin B, Ermentrout G, Reyes A. Phase-response curves give the responses of neurons to transient inputs. Journal of Neurophysiology 2004;94:1623–1635. [PubMed: 15829595]

Jeong H, Gutkin B. Synchrony of neuronal oscillations controlled by gabaergic reversal potentials. Neural Computation 2007;19:706–729. [PubMed: 17298230]

Kurths, J.; Pikovsky, A.; Rosenblum, M. Synchronization, a universal concept in non-linear science. Cambridge University Press; 2001.

LeBeau F, Towers S, Traub R, Whittington M, Buhl E. Fast network oscillations induced by potassium transients in the rat hippocampus *in vitro*. Journal of Physiology 2002;542:167–179. [PubMed: 12096059]

Mann E, Suckling J, Hajos N, Greenfield S, Paulsen O. Perisomatic feedback inhibition underlies cholinergically induced fast network oscillations in the rat hippocampus *in vitro*. Neuron 2005;45:105–117. [PubMed: 15629706]

Maran S, Canavier C. Using phase resetting to predict 1:1 and 2:2 locking in two neuron networks in which firing order is not always preserved. Journal of Computational Neuroscience 2008;24:37–55. [PubMed: 17577651]

Mima T, Oluwatimilehin T, Hiraoka T, Hallett M. Transient interhemispheric neuronal synchrony correlates with object recognition. The Journal of Neuroscience 2001;21:3942–3948. [PubMed: 11356882]

Murray, J. Mathematical biology. Springer Verlag; Berlin: 1993.

Oprisan S, Canavier C. Stability analysis of ring of pulse coupled oscillators: The effect of phase resetting in the second cycle after the pulse is important at synchrony and for long pulses. Differential Equations and Dynamical Systems 2001;9:243–258.

Oprisan S, Prinz A, Canavier C. Phase resetting and phase locking in hybrid circuits of one model and one biological neuron. Biophysical Journal 2004;87:2283–2298. [PubMed: 15454430]

Sejnowski, T. Open questions about computation in cerebral cortex. MIT Press; Cambridge: 1986.

Strogatz, S. Nonlinear dynamics and chaos with application to physics, biology, chemistry and engineering. Westview Press; 2001.

Talathi S, Hwang D, Ditto W. Spike timing dependent plasticity promotes synchrony of inhibitory networks in the presence of heterogeneity. Journal of Computational Neuroscience 2008;25:262–281. [PubMed: 18297384]

Talathi S, Hwang D, Miliotis A, Carney P, Ditto W. Predicting synchrony in heterogeneous pulse coupled oscillators. Physical Review E 2009;80:021908.

vanVreeswijk C, Abbott L, Ermentrout B. When inhibition and not excitation synchronizes neural firing. Journal of Computational Neuroscience 1994;1:313–321. [PubMed: 8792237]

Vida I, Bartos M, Jonas P. Shunting inhibition improves robustness of gamma oscillations in hippocampal interneuron networks by homogenizing firing rates. Neuron 2006;49:107–117. [PubMed: 16387643]

Wang X, Buzsaki G. Gamma oscillation by synaptic inhibition in a hippocampal interneuronal network model. The Journal of Neuroscience 1996;16:6402–6413. [PubMed: 8815919]

Wang X, Rinzel J. Alternating and synchronous rhythms in reciprocally inhibitory model neurons. Neural Computation 1992;4:84–97.

White A, Chow C, Ritt J, Trevino C, Kopell N. Synchronization and oscillatory dynamics in heterogeneous, mutually inhibited neurons. Journal of Computational Neuroscience 1998;5:5–16. [PubMed: 9580271]

Whittington M, Traub R, Jefferys J. Synchronized oscillations in interneuron networks driven by metabotropic glutamate receptor activation. Nature 1995;373:612–615. [PubMed: 7854418]

Winfree, A. The geometry of biological time. 2. NY: Springer Verlag; 2001.

Wolf F, Geisel T. Neurophysics:logic gates come to life. Natural Physique 2008;4:905–906.

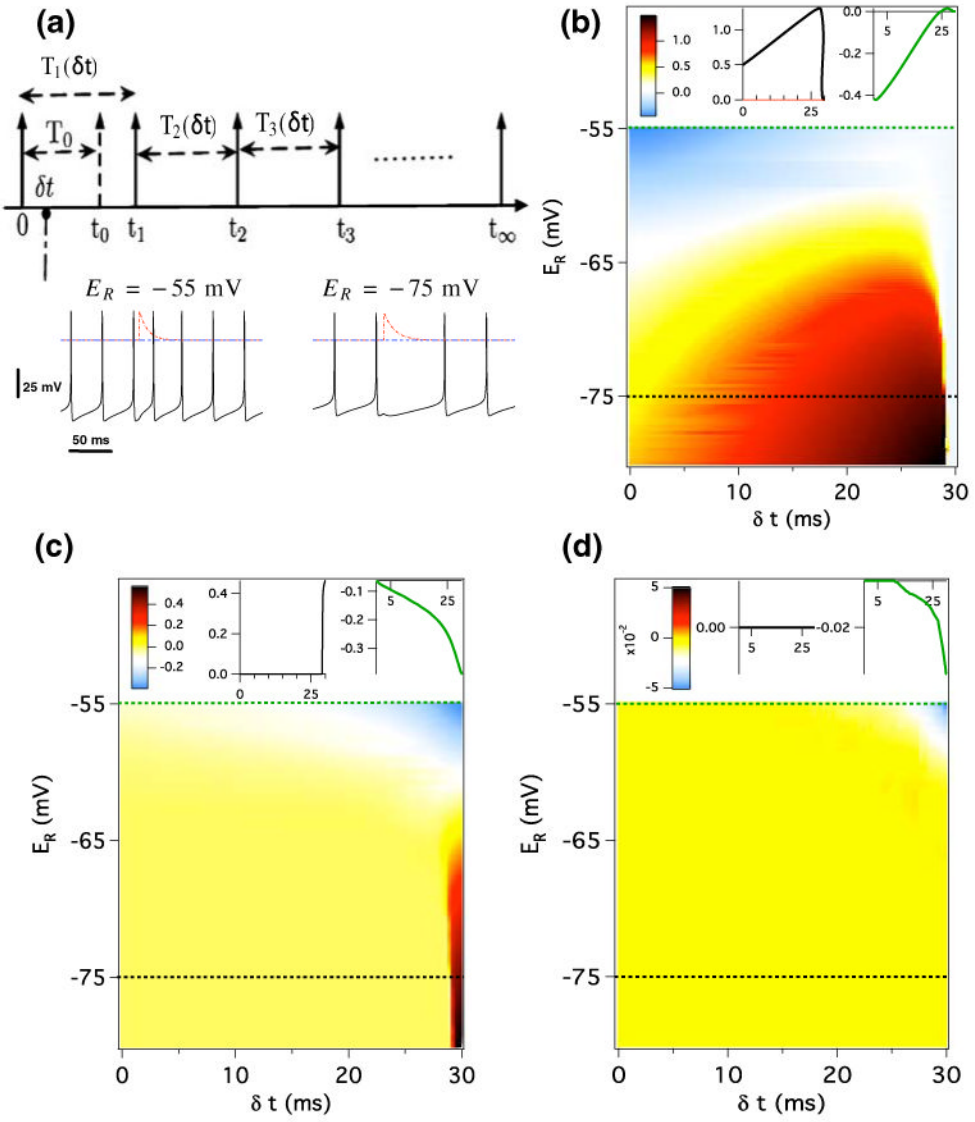

Fig. 1.

(**a**) Schematic diagram for STRC calculations. The neuron firing with intrinsic period T_0 = 31 ms receives a single synaptic perturbation at time δt. as a result subsequent firing cycles are affected. Depending on the type of synapse and the synaptic kinetics, the effect of perturbation can persist for multiple firing cycles, resulting in $T_j(\delta t) \neq T_0$ (j = 1,2,3…). Inset to Fig. 1(a) (below the schematic diagram) we show the actual time series for membrane potential of a neuron receiving a single synaptic perturbation through a shunting synapse (E_R = −55 mV) and hyperpolarizing synapse (E_R = −75 mV) respectively. We see that the shunting synapse shortens the effective period of the firing cycle in which the perturbation is received, such that there is still significant non-zero synaptic contribution (the red trace showing $S(t)$) which affects the subsequent firing cycle. However for hyperpolarizing synapse, the perturbation prolongs the length of first cycle such that synaptic contribution is essentially zero in the following cycle. (**b**) First order STRC Φ_1 is color coded as function of the reversal potential of the inhibitory synapse and the perturbation time. (**c**) Second order STRC Φ_2 is color coded as function of the reversal potential of the inhibitory synapse and the perturbation time. (**d**) The third order STRC Φ_3 is color coded as function of the reversal

potential of the inhibitory synapse and the perturbation time. Inset of Fig. 1(b–d) show the STRC's calculated for two specific cases corresponding to a hyperpolarizing synapse (E_R = −75 mV, shown in black) and a shunting synapse (E_R = −55 mV, shown in green). The synaptic parameters are g_s = 0.15 mS/cm^2, τ_R = 0.1 ms, τ_D = 8 ms. The resting potential of the neuron is V_{rest} = −65 mV (I^{DC} = 0) and the threshold to spiking is $V_T \approx -55$mV

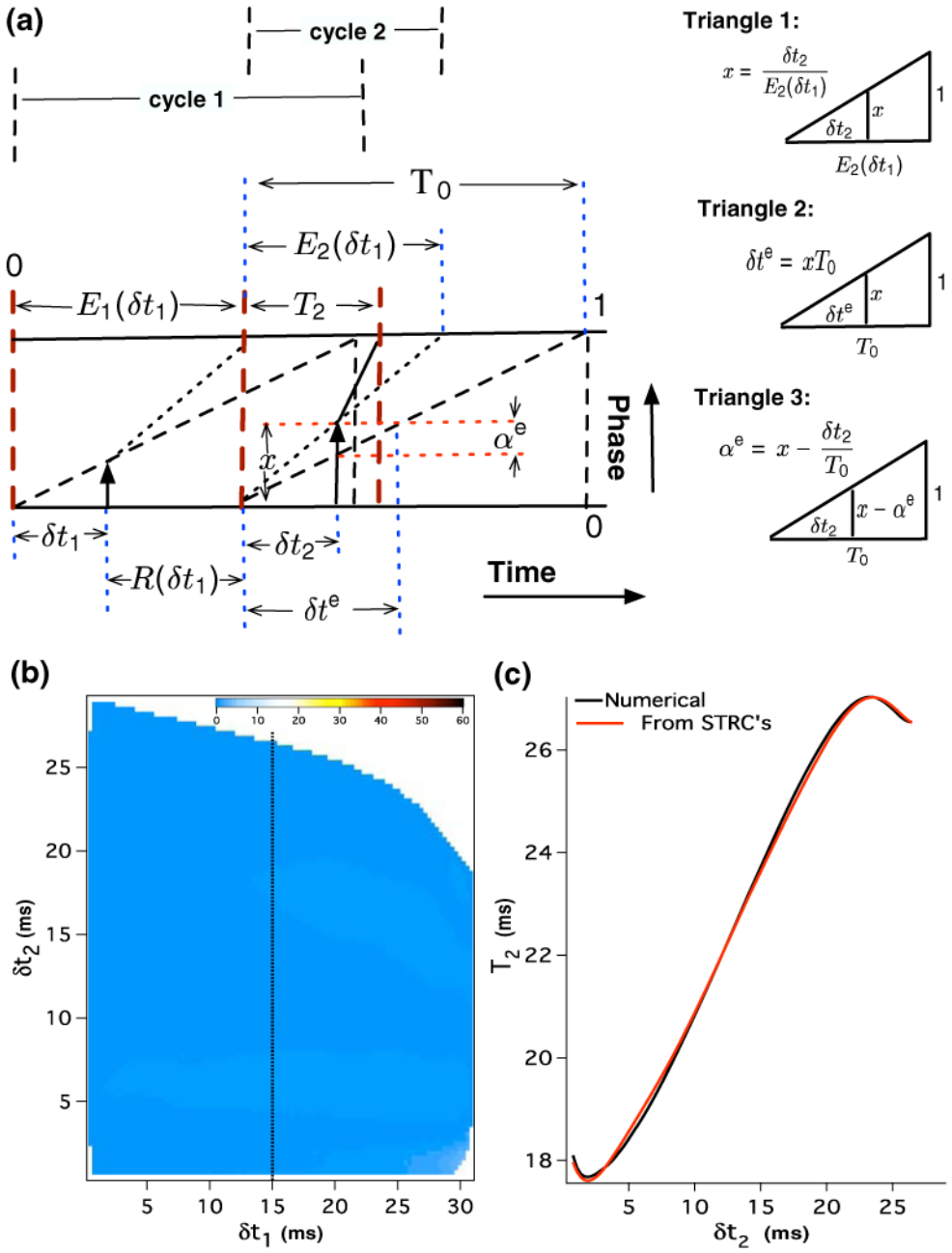

Fig. 2.

(**a**) Schematic diagram of the re-normalization and the re-scaling procedure to determine the length of second cycle $T_2(\delta t_1, \delta t_2)$ (adapted from Talathi et al. (2009)). Red dashed lines represents the effective spike times after the neuron receives two consecutive synaptic perturbations. Black dotted lines represent the change in the firing cycle caused by synaptic input in the first firing cycle. Shown in black dashed line is the unperturbed firing cycle for the neuron. To the right (inset to Fig. 2(a)) we shown three distinct triangles that can be extracted from Fig. 2(a), which are used to determine the re-normalized effective synaptic perturbation time δt^e and the re-scaled amplitude of the phase of synaptic perturbation α^e (**b**) The percent error δE_2 between the numerically estimated value T_2^N and the analytically

estimated value T_2^P through Eq. (4) for the second cycle $T_2(\delta t_1, \delta t_2)$ is color coded as function of the synaptic perturbation times δt_1 and δt_2. (**c**) The numerically estimated period T_2^N (shown in black) and the analytically estimated period T_2^P for a given value of first perturbation time $\delta t_1 = 15$ ms is plotted as function of the second synaptic perturbation time. The synaptic parameters are $g_s = 0.15$ mS/cm^2, $\tau_R = 0.1$ ms, $\tau_D = 8$ ms and $E_R = -55$ mV. The intrinsic period $T_0 = 31$ ms

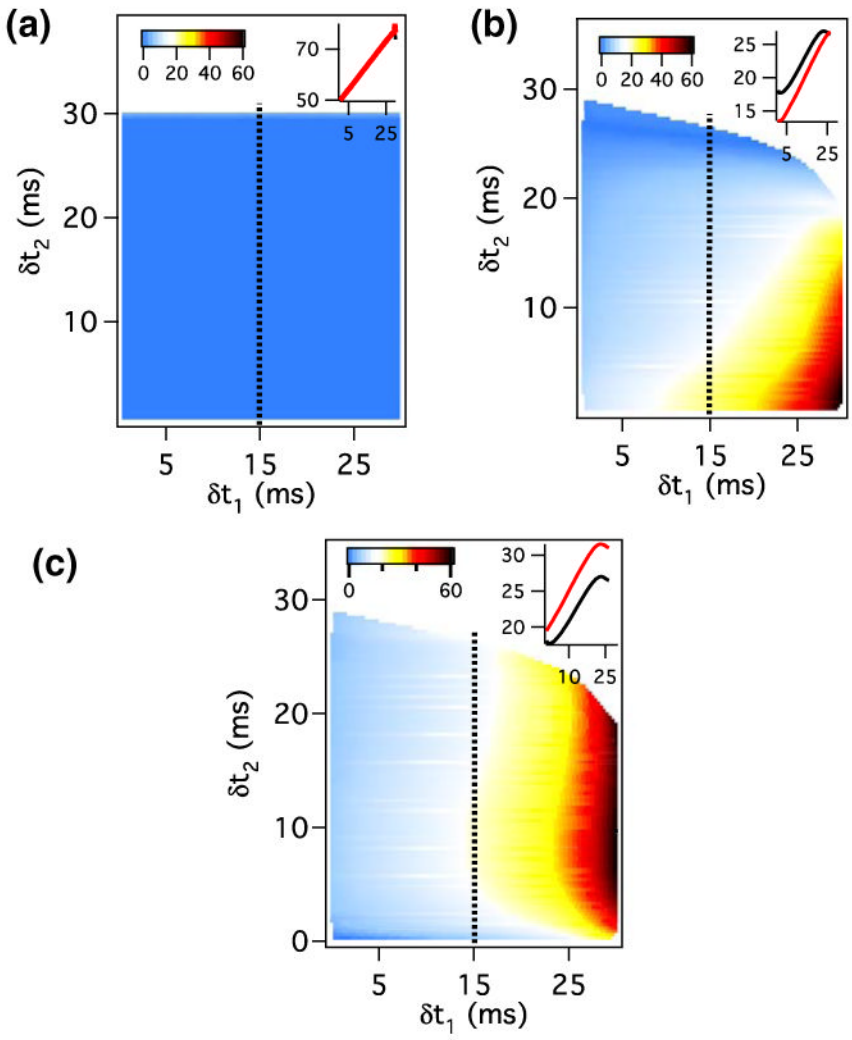

Fig. 3.

(**a**) Color coded percent error δE_2 between the numerically estimated period T_2^N and the analytically determined period T_2^P through Eq. (5) for a neuron receiving two consecutive synaptic inputs through a hyperpolarizing synapse with parameters $E_R = -80$ mV, $g_s = 0.15$ mS/cm^2, $\tau_R = 0.1$ ms, and $\tau_D = 8$ ms. (**b**) Color coded percent error δE_2 determine through Eq. (5) for the neuron receiving two synaptic inputs through a shunting synapse with synaptic parameters $g_s = 0.15$ mS/cm^2, $\tau_R = 0.1$ ms, $\tau_D = 8$ ms and $E_R = -55$ mV. (**c**) Color coded percent error δE_2 determine through Eq. (6) for the neuron receiving two synaptic inputs through a shunting synapse with synaptic parameters $g_s = 0.15$ mS/cm^2, $\tau_R = 0.1$ ms, $\tau_D = 8$ ms and $E_R = -55$ mV.) The inset in each of the Fig. 3(a–c) shows the plot of $T_2(\delta t_1, \delta t_2)$ as a function of second perturbation time δt_2 for a fixed value for the time of first synaptic perturbation at $\delta t_1 = 15$ ms. Numerical estimate is shown in black and the analytically determined period is shown in red

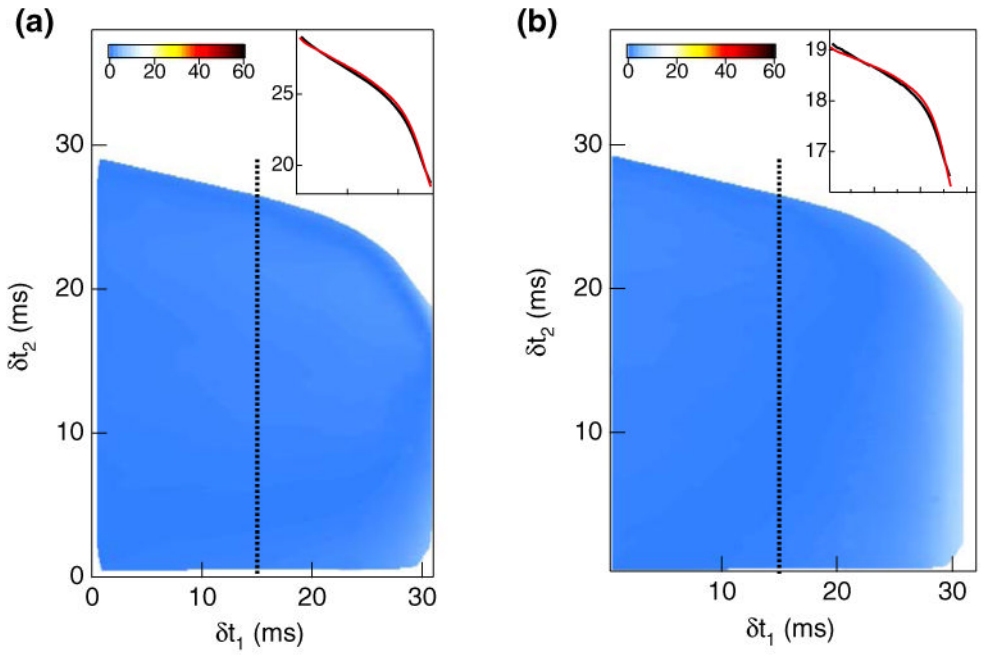

Fig. 4.

(**a**) Color coded percent error $\delta\tilde{E}_3$ between the predicted value $\tilde{E}_3^P$ and the numerically estimated value $\tilde{E}_3^N$ for the length of third cycle $\tilde{E}_3$ in the presence of two consecutive synaptic inputs at times δt_1 and δt_2 respectively. The inset shows the variation in $\tilde{E}_3$ ($\tilde{E}_3^N$ shown in black and $\tilde{E}_3^P$) shown in red) as a function of δt_2 for δt_1 = 15 ms. (**b**) Color coded percent error δE_3 between the predicted value T_3^P and the numerically estimated value T_3^N for the length of third cycle T_3 in the presence of three consecutive synaptic inputs at times δt_1, δt_2 and δt_3 = 5 ms respectively. The inset shows the variation in $T_3(\delta t_1, \delta t_2, \delta t_3)$ (T_3^N shown in black and T_3^P) shown in red) as a function of δt_2 for δt_1 = 15 ms and δt_3 = 15 ms. The synaptic parameters are g_s = 0.15 mS/cm^2, τ_R = 0.1 ms, τ_D = 8 ms and E_R = −55 mV

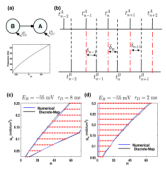

Fig. 5.

(**a**) Schematic diagram of the unidirectionally coupled pair of interneurons A and B. Also shown is the variation in the intrinsic firing frequency of the neuron as function of percent heterogeneity H, defined as $H=100\frac{I_{DC}-0.5}{0.5}$ where I_{DC} is the input current to the neuron. (**b**) Schematic diagram of spike times for neurons A and B, when they are phase locked in 1:1 synchrony. (**c**) Arnold tongue representing the domain for 1:1 synchrony in the UCI network in the two-dimensional $g_s - H$ plane, is shown in black (determined through stable fixed point solutions to Eq. (9)) and shown in blue (computed through numerical simulations). The synaptic parameters are τ_R = 0.1 ms, τ_D = 8 ms and E_R = −55 mV, representing a slow shunting synapse. (**d**) Arnold tongue for the UCI network interacting through a fast shunting synapse with synaptic parameters τ_R = 0.1 ms, τ_D = 2 ms and E_R = −55 mV

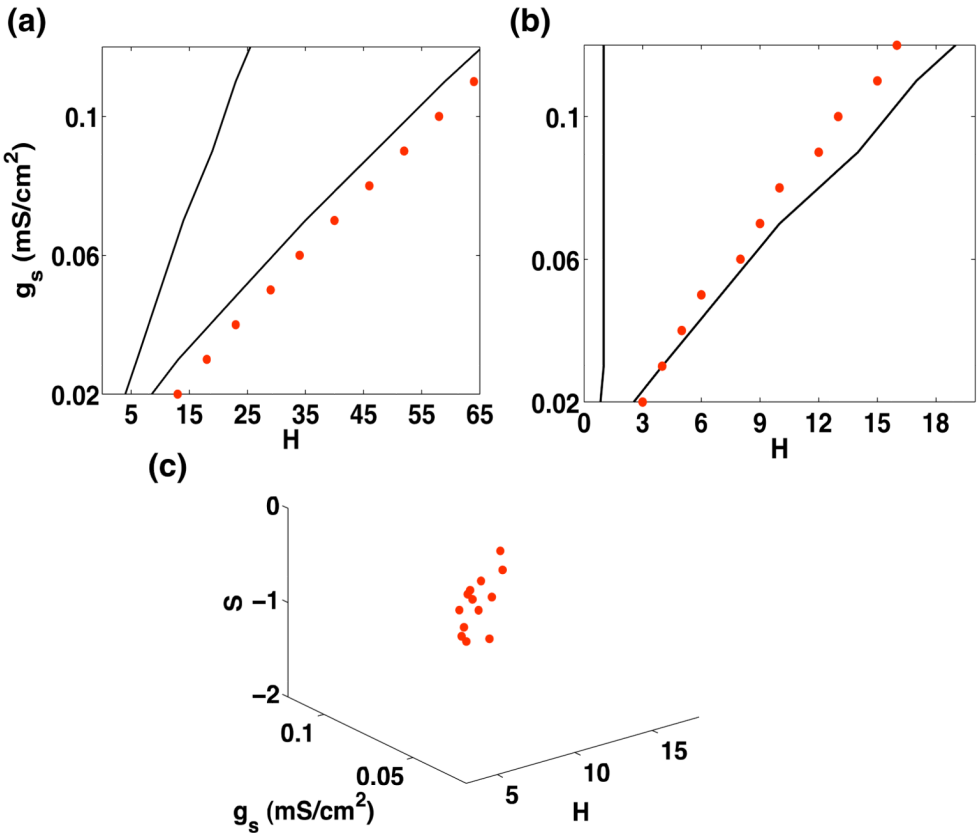

Fig. 6.

(**a**) Arnold tongue for the UCI network with slow shunting synapse. (**b**) Arnold tongue for the UCI network with fast shunting synapse. The red dotted circles in a-b represent points that satisfy Eq. (11) corresponding to fixed point solution $\delta^* = 0$ for the discrete map in Eq. (9). (c) The red circles represent values for the function S in Eq. (12), calculated at points that represent the solution to Eq. (11) for the UCI network with fast shunting synapse

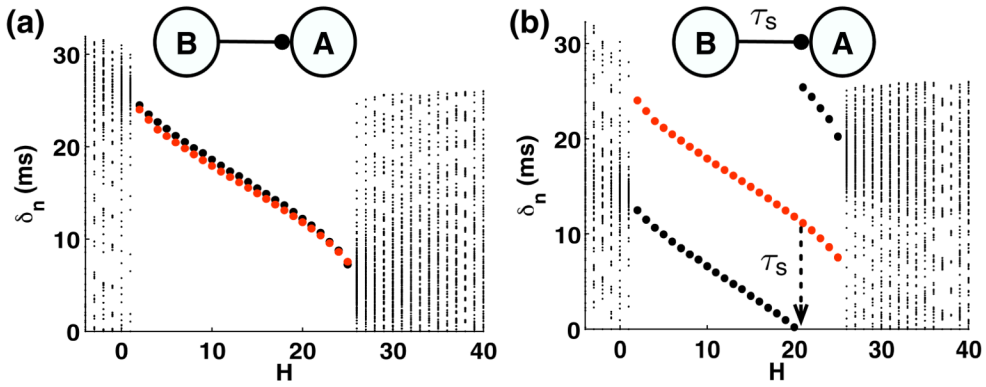

Fig. 7.

The time lag δ_n between spike times of the two neurons in the UCI network coupled through a fast shunting synapse (**a**) without synaptic delay and (**b**) with synaptic delay τ_s = 12 ms. The small dotted circles correspond to the situation when the two neurons are not phase locked in 1:1 synchrony representing the state of asynchronous oscillations between the two neurons. The black bold circles correspond to the value of δ_n obtained numerically in the region within the Arnold tongue when the two neurons are phase locked in 1:1 synchrony. The red circles represent the solution to Eq. (10) corresponding to the stable fixed point's of the discrete map in Eq. (9)

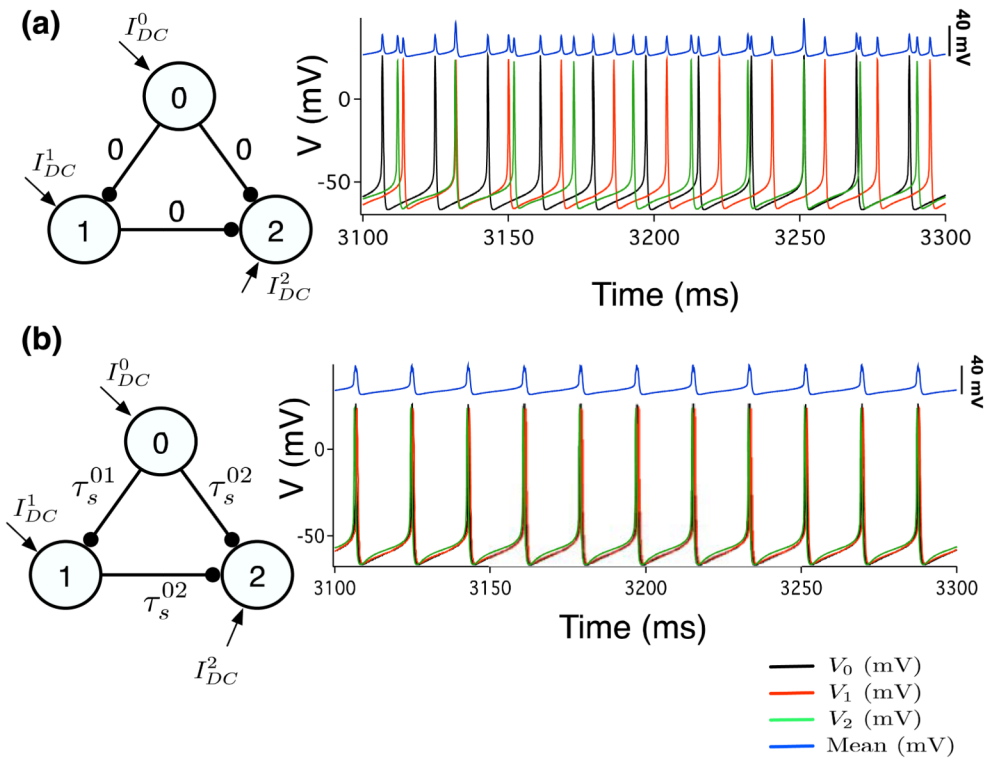

Fig. 8.

(**a**) Feed-forward network of three heterogeneously firing interneurons coupled through a slow shunting synapse in absence of any synaptic delay. (**b**) Feed-forward network of three heterogeneously firing interneurons coupled through a slow shunting synapse with synaptic delay τ_s^{ij} (i, j=0, 1, 2). The membrane potential of neuron 0,1 and 2 is shown in colors black, red and green respectively. The mean membrane potential is shown in blue trace. The constant input current values are I^0_{DC}=0.9113 μA/cm^2, I^1_{DC}=0.675 μA/cm^2, I^2_{DC}=0.5 μA/cm^2. The synaptic delay determined from the fixed point solution to the discrete map in Eq. (11) are τ_s^{01}=12.16 ms and τ_s^{02}=1.98 ms. The synaptic parameters are: g_s = 0.15 mS/cm^2, τ_R = 0.1 ms, τ_D = 8 ms and E_R = −55 mV